Coded Modulation Assisted Radial Basis Function Aided Turbo Equalization for Dispersive Rayleigh-Fading Channels

Soon Xin Ng, Mong-Suan Yee, and Lajos Hanzo, *Fellow, IEEE*

Abstract—In this contribution a range of coded modulation (CM)-assisted radial basis function (RBF)-based turbo equalization (TEQ) schemes are investigated when communicating over dispersive Rayleigh-fading channels. Specifically, 16 quadrature amplitude modulation-based trellis coded modulation (TCM), turbo TCM (TTCM), bit-interleaved coded modulation (BICM), and iteratively decoded BICM (BICM-ID) are evaluated in the context of an RBF-based TEQ scheme and a reduced-complexity RBF based in-phase/quadrature-phase (I/Q) TEQ scheme. The least mean square (LMS) algorithm was employed for channel estimation, where the initial estimation step-size used was 0.05, which was reduced to 0.01 for the second and the subsequent TEQ iterations. The achievable coding gain of the various CM schemes was significantly increased, when employing the proposed RBF-TEQ or RBF-I/Q-TEQ rather than the conventional noniterative decision feedback equalizer (DFE). Explicitly, the reduced-complexity RBF-I/Q-TEQ-CM achieved a similar performance to the full-complexity RBF-TEQ-CM, while attaining a significant complexity reduction. The best overall performer was the RBF-I/Q-TEQ-TTCM scheme, requiring only 1.88 dB higher signal-to-noise ratio at $\mathrm{BER} = 10^{-5}$, than the identical throughput 3 b/symbol uncoded 8 PSK scheme communicating over an additive white Gaussian noise channel. The coding gain of the scheme was 16.78 dB.

Index Terms—Bit-interleaved coded modulation (BICM), iteratively decoded BICM (BICM-ID), coded modulation (CM), in-phase/quadrature-phase (I/Q), radial basis function (RBF), trellis coded modulation (TCM), turbo equalization (TEQ), turbo TCM (TTCM).

I. INTRODUCTION

S PECTRAL efficiency is of primary concern in mobile communication systems owing to the scarcity and high price of the radio spectrum available for mobile radio services. In an effort to efficiently exploit the available spectrum, coded modulation (CM) schemes, which are based on combining the functions of channel coding and modulation, were proposed [1], [2]. In this contribution, trellis coded modulation (TCM) [1], [2], turbo TCM (TTCM) [1], [3], bit-interleaved coded modulation (BICM) [1], [4], [5], and iteratively decoded BICM (BICM-ID) [1], [6] will be studied. Furthermore, channel equalization is

The authors are with the Department of Electrical and Computer Science, University of Southampton, Hampshire SO17 1BJ, U.K. (e-mail: lh@ecs.soton.ac.uk).

invoked for mitigating the effects of intersymbol interference (ISI) in the context of single carrier modulation, when communicating over frequency selective channels.

A radial basis function (RBF)-based equalizer [7] constitutes a nonlinear equalization scheme, which formulates the channel equalization procedure as a classification problem. More explicitly, in conventional equalizers [8], [9] the received signal is linearly filtered with the aid of the channel equalizer, which aims to mimic the inverse of the channel's impulse response (CIR). By contrast, given the CIR, the RBF-based equalizer determines all possible channel outputs engendered by the set of legitimate transmitted symbols and then classifies each received symbol into the nearest legitimate channel output, which allows us to infer the specific symbol transmitted. The application of nonlinear RBF-based equalizers has been studied in conjunction with channel codecs [10], [11], space-time codes [12] as well as turbo equalization (TEQ) [13]. The bit-error ratio (BER) performance of RBF-based TEQ presented in [13] was found to be similar to that of conventional trellis-based TEQ (CT-TEQ) [14] employing a log-MAP equalizer in the context of quadrature amplitude modulation (QAM), although CT-TEQ performs better than RBF-TEQ during the first turbo iteration. The RBF-assisted TEQ schemes are however capable of maintaining a lower complexity than their conventional trellis-based counterparts, when communicating over both dispersive Gaussian- and Rayleigh-fading channels, while maintaining a similar performance, after a few turbo iterations. The complexity of the RBF-TEQ scheme can be further reduced by invoking the in-phase/quadrature-phase turbo equalization (I/Q-TEQ) technique, while maintaining a similar performance to that of the CT-TEQ [11]. Explicitly, the philosophy of carrying out the equalization of the in-phase and quadrature-phase components separately is appealing, since the dimensionality of the I and Q components is significantly lower than that of the complex constellation, which reduces the equalizer's complexity. However, this principal can only be invoked in conjunction with TEQ where the associated gross simplification of considering the I and Q components in isolation and, hence, disregarding their channel-induced cross-coupling is compensated by the turbo-equalizer's consecutive iterations [1].

The rest of this paper is organized as follows. The TEQ scheme utilizing a symbol-based MAP decoder is introduced in Section II and a novel RBF-TEQ based CM scheme is presented in Section III. The reduced-complexity I/Q-TEQ philosophy is introduced in Section IV, while a reduced complexity

RBF-I/Q-TEQ based CM scheme is proposed in Section V. Finally, we will offer our conclusions in Section VI.

II. TURBO EQUALIZATION USING SYMBOL-BASED MAP DECODER

In a noniterative RBF equalizer-based system channel equalization and channel decoding are performed independently. However, it is possible to improve the receiver's performance, if the equalizer is fed by the channel outputs plus the soft decisions provided by the channel decoder, invoking a number of iterative processing steps. This novel receiver scheme was first proposed by Douillard *et al.* [15] for a convolutional coded binary phase shift keying (BPSK) system, using a similar principle to that of turbo codes and, hence, it was termed TEQ [1]. This scheme is illustrated in Fig. 1, which will be detailed during our forthcoming discourse. Gertsman and Lodge [16] extended this work and showed that the iterative process of TEQ is capable of compensating for the performance degradation imposed by imperfect channel estimation. In [17], TEQ was implemented in conjunction with turbo coding, rather than conventional convolutional coding, by Raphaeli and Zarai, which demonstrated an increased performance gain owing to turbo coding as well as with the advent of enhanced ISI mitigation achieved by TEQ.

A. Principle of TEQ Using Symbol-Based MAP Decoder

The principles of bit-based iterative turbo decoding [18] were modified appropriately for employment of the symbol-based M-ary coded modulation system of Fig. 2. As seen in the figure, a data symbol d_n is fed into the channel encoder in order to yield a channel encoded symbol c_n of $\mathsf{m} = \log_2(\mathsf{M})$ bits. The interleaved channel encoded symbol c_k is mapped to an M-ary symbol before transmission. In this scheme, the channel is viewed as an "inner encoder" of a serially concatenated arrangement, since it can be modeled with the aid of a tapped delay line similar to that of a convolutional encoder [15], [19], as it was also demonstrated in [11, Sec. 16.5]. At the receiver, the equalizer and decoder employ a soft-in soft-out (SISO) algorithm, such as the optimal maximum *a posteriori* (MAP) algorithm [1], [20] or the log-MAP algorithm [1], [21]. The SISO equalizer processes the *a priori* information associated with the coded symbol c_k transmitted over the channel and—in conjunction with the channel output values v_k—computes the *a posteriori* information concerning the coded symbol. The soft values of the coded bits constituting the channel coded symbol c_k are normally quantified in the form of a log-likelihood ratio [15]. However, here we will quantify them in the form of the symbol probabilities using the symbol-based MAP decoder [1], [3]. Note that in the context of TEQ, the *a posteriori* information concerning all the *coded* bits is required, whereas in the context of conventional turbo channel decoding, only the *a posteriori* information of the information bits are computed.

In our description of the turbo equalizer depicted in Fig. 1, we have used the notation $\mathcal{L}^E$ and $\mathcal{L}^D$ for denoting the log-domain probability (LP) values output by the SISO equalizer and SISO decoder, respectively. The subscripts e, i, a, and p were used to represent the extrinsic LP, the combined channel and extrinsic
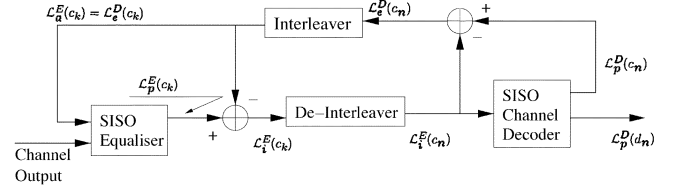

Fig. 1. Iterative TEQ schematic.

LP, the *a priori* LP and the *a posteriori* LP, respectively. Referring to Fig. 1, the SISO equalizer processes the channel outputs and the *a priori* information $\mathcal{L}_a^E(c_k)$ of the coded symbol, and generates the *a posteriori* LP values $\mathcal{L}_p^E(c_k)$ of the interleaved coded symbol c_k seen in Fig. 2. Before passing, the *a posteriori* LPs generated by the SISO equalizer to the SISO decoder of Fig. 1, the contribution of the decoder—which is represented in the form of the *a priori* information $\mathcal{L}_a^E(c_k)$—accruing from the previous iteration must be removed, in order to yield the combined channel and extrinsic information $\mathcal{L}_i^E(c_k)$ seen in Fig. 1. To expound a little further, the channel and extrinsic information are referred to as "combined," since they are intrinsically bound and cannot be separated. However, note that at the initial iteration stage no *a priori* information is available yet. To elaborate further, the *a priori* information $\mathcal{L}_a^E(c_k)$ was removed at this stage, in order to prevent the decoder from processing its own output information, which would result in overwhelming the decoder's current reliability-estimation characterising the coded bits, i.e., the extrinsic information. The combined channel and extrinsic LP values are channel-deinterleaved—as seen in Fig. 1—in order to yield $\mathcal{L}_i^E(c_n)$ which is then passed to the SISO channel decoder. Subsequently, the channel decoder computes the *a posteriori* LP values $\mathcal{L}_p^D(c_n)$ of the coded symbol. The *a posteriori* LP's generated at the output of the channel decoder consists of the extrinsic LP $\mathcal{L}_e^D(c_n)$ and the channel-deinterleaved combined channel and extrinsic LP $\mathcal{L}_i^E(c_n)$ extracted from the equalizer's *a posteriori* LP $\mathcal{L}_p^E(c_k)$. The extrinsic part can be interpreted as the incremental information concerning the current symbol obtained through the decoding process from all the information available due to all surrounding symbols imposed by the code constraints, but excluding the information directly conveyed by the symbol. This information can be calculated by subtracting on a symbol-by-symbol basis the LP values $\mathcal{L}_i^E(c_n)$ at the input of the decoder from the *a posteriori* LP values $\mathcal{L}_p^D(c_n)$ at the channel decoder's output, as seen also in Fig. 1 TEQ, yielding

$$\mathcal{L}_e^D(c_n) = \mathcal{L}_p^D(c_n) - \mathcal{L}_i^E(c_n). \qquad (1)$$

The extrinsic information $\mathcal{L}_e^D(c_n)$ of the coded symbol is then interleaved as shown in Fig. 1, in order to yield $\mathcal{L}_e^D(c_k)$, which is fed back in the required symbol-order to the channel equalizer, where it is used as the *a priori* information $\mathcal{L}_a^E(c_k)$ in the next equalization iteration. This constitutes the first iteration. Again, it is important that only the channel-interleaved extrinsic part—i.e. $\mathcal{L}_e^D(c_k)$ of $\mathcal{L}_p^D(c_n)$—is fed back to the equalizer, since the interdependence between the *a priori* information $\mathcal{L}_a^E(c_k) = \mathcal{L}_e^D(c_k)$ used by the equalizer and the previous decisions of the equalizer should be minimized. This independence assists in obtaining the equalizer's reliability-estimation of the
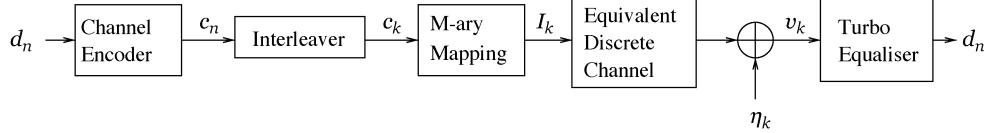
Fig. 2.   Serially concatenated coded M-ary system using the turbo equalizer, which performs the equalization, demodulation and channel decoding iteratively.

coded symbols for the current iteration, without being "influenced" by its previous estimations. Ideally, the *a priori* information should be based on an independent estimation. As argued earlier, this is the reason that the *a priori* information $\mathcal{L}_a^E(c_k)$ is subtracted from the *a posteriori* LP value $\mathcal{L}_p^E(c_k)$ at the output of the channel equalizer in Fig. 1, before passing the LP values to the channel decoder. In the final iteration, the *a posteriori* LPs $\mathcal{L}_p^D(d_n)$ of the information symbols are computed by the channel decoder.

Previous TEQ research has implemented the SISO equalizer using the soft-output viterbi algorithm (SOVA) [15], the optimal MAP algorithm [14], and linear filters [22]. We will now introduce the RBF based equalizer as the SISO equalizer, which will be employed in the context of TEQ using the symbol-based MAP algorithm.

III. RBF ASSISTED TEQ OF CODED MODULATION SCHEMES

The RBF network-based equalizer is capable of utilising the *a priori* information $\mathcal{L}_a^E(c_k)$ provided by the channel decoder of Fig. 1, in order to improve its performance. This *a priori* information can be assigned namely to the weights of the RBF network [23]. In turn, the RBF equalizer provides the decoder with the *a posteriori* information $\mathcal{L}_p^E(c_k)$ concerning the coded symbol. We will now provide a brief overview of symbol-based coded modulation assisted, RBF aided TEQ. Note that this procedure is different from the separate bit-based channel coding and modulation philosophy outlined in [11, Sec. 11.2].

A. System Overview

The conditional probability density function (pdf) of the ith symbol, $i = 1, \ldots, M$, associated with the ith subnet of the M-ary RBF channel equalizer having a feedforward order of m is given by [11]

$$f_{RBF}^i(\mathbf{v_k}) = \sum_{j=1}^{n_{s,i}} P\left(\mathbf{r_j^i}\right) \left(2\pi\sigma_N^2\right)^{-\frac{m}{2}} \exp\left(\frac{-\left|\mathbf{v_k} - \mathbf{r_j^i}\right|^2}{2\sigma_N^2}\right)$$

$$i = 1, \ldots, M, \quad j = 1, \ldots, n_{s,i} \quad (2)$$

where

$$w_j^i = P\left(\mathbf{r_j^i}\right) \left(2\pi\sigma_N^2\right)^{-\frac{m}{2}} \quad (3)$$

is the RBF's weight and

$$\varphi(x) = \exp\left(\frac{-x^2}{2\sigma_N^2}\right) \quad (4)$$

is the activation function [11]. Furthermore, $\mathbf{r_j^i}$ are the RBF's centers, which are assigned the values of the channel output states in order to arrive at the Bayesian equalization solution [11], [24], $\mathbf{v_k}$ is the received symbol sequence and σ_N^2 is the noise variance of the channel. The actual number of channel states $n_{s,i}$ is determined by the specific design of the algorithm invoked, but in general, we aim for reducing the number of

channel states from the optimum number of $n_{s,i} = M^{m+\bar{L}-1}$, where m is the equalizer feedforward order and $\bar{L}+1$ is the CIR duration [25]–[27], to a lower value for the sake of reducing computational complexity.

The term $\mathbf{v_k}$ in (2) is the received symbol sequence, as shown in Fig. 2. Explicitly, $\mathbf{v_k}$ consists of the channel outputs observed by the mth order equalizer, which can be expressed in an m-dimensional vectorial form as

$$\mathbf{v_k} = \begin{bmatrix} v_k & v_{k-1} & \ldots & v_{k-m+1} \end{bmatrix}^{\mathbf{T}}. \quad (5)$$

The channel input state associated with the ith subnet of the M-ary RBF channel equalizer is given by the vector $\mathbf{s_j^i}$, which is also referred to as the channel input vector. Explicitly, this vector consists of the jth possible combination of the $(\bar{L}+m)$ number of transmitted symbols, namely by

$$\mathbf{s_j^i} = \begin{bmatrix} s_{j1} & \ldots & s_{j(\tau+1)} = g(i) & \ldots & s_{jp} & \ldots & s_{j(\bar{L}+m)} \end{bmatrix}^{\mathbf{T}} \quad (6)$$

where τ is the equalizer's decision delay and $g(i)$ translates the ith M-ary symbol to the complex plane. The channel output state $\mathbf{r_j^i}$ associated with the ith subnet of the M-ary RBF channel equalizer is the product of the CIR matrix $\mathbf{H}$ and the channel input states $\mathbf{s_j^i}$. The variable $\mathbf{r_j^i}$ is also referred to as the channel output vector and it is expressed as [11]

$$\mathbf{r_j^i} = \mathbf{Hs_j^i} \quad (7)$$

where the z-transform of the CIR $h(t)$ having a memory of $\bar{L}$ symbols is represented by $H(z) = \sum_{n=0}^{\bar{L}} h_n z^{-n}$ and $\mathbf{H}$ is an $m \times (m + \bar{L})$ matrix given by the CIR taps as follows:

$$\mathbf{H} = \begin{bmatrix} h_0 & h_1 & \ldots & h_{\bar{L}} & \ldots & 0 \\ 0 & h_0 & \ldots & h_{\bar{L}-1} & \ldots & 0 \\ \vdots & \vdots & & & & \vdots \\ 0 & \ldots & h_0 & \ldots & h_{\bar{L}-1} & h_{\bar{L}} \end{bmatrix}. \quad (8)$$

The RBF weights w_j^i correspond to the *a priori* probability of the channel states $P(\mathbf{r_j^i})$, $i = 1, \ldots, M$, $j = 1, \ldots, n_{s,i}$, as shown in (3). The probability of the channel states $P(\mathbf{r_j^i})$ and, therefore, the weights of the RBF equalizer can be derived from the *a priori* information $\mathcal{L}_a^E(c_k)$ estimated by the symbol-based MAP channel decoder. Explicitly, $\mathcal{L}_a^E(c_k)$ is the interleaved version of the extrinsic information $\mathcal{L}_e^D(c_n)$ in (1). Based on (7), assuming a time-invariant CIR and that the symbols in the sequence $\mathbf{s_j^i}$ are statistically independent of each other with the advent of using the interleaver, the probability of the received channel output states $\mathbf{r_j^i}$ is given by

$$P\left(\mathbf{r_j^i}\right) = P\left(\mathbf{s_j^i}\right)$$
$$= P\left(s_{j1} \cap \ldots s_{j(\tau+1)} = g(i) \cap \ldots s_{jp} \cap \ldots s_{j(\bar{L}+m)}\right)$$
$$= \prod_{p=1}^{\bar{L}+m} P(s_{jp})$$
$$= \prod_{p=1}^{\bar{L}+m} \exp\left(\mathcal{L}_a^E(s_{jp} = c_{k-p+1})\right), \quad j = 1, \ldots, n_{s,i} \quad (9)$$

where the transmitted symbol vector component s_{jp}, i.e., the pth symbol in the vector of (6), is given by $m = \log_2 M$ number of bits $b_{jp1}, b_{jp2}, \ldots, b_{jpm}$, which constitute the coded symbol c_{k-p+1}. Explicitly, the transmitted symbol vector component s_{jp} is mapped to the coded symbol c_{k-p+1}.

In summary, the computation of the pdf $f^i_{RBF}(\mathbf{v_k})$ of the ith symbol in (2), $i = 1, \ldots, M$, which is associated with the ith subnet of the M-ary RBF channel equalizer, requires the knowledge of the channel states' *a priori* probability $P(\mathbf{r^i_j})$, when determining the RBF weights w^i_j, as shown in (3). Finally, $P(\mathbf{r^i_j})$ can be computed from (9) using the **a priori** information $\mathcal{L}^E_a(c_k)$. Explicitly, $\mathcal{L}^E_a(c_k)$ is the interleaved version of the extrinsic information $\mathcal{L}^D_e(c_n)$ of (1), and the *a posteriori* information $\mathcal{L}^D_p(c_n)$ is obtained from the channel decoder. Therefore, we have demonstrated how the soft output $\mathcal{L}^E_a(c_k)$ provided by the symbol-based MAP channel decoder of Fig. 1 can be utilized by the RBF equalizer.

On the other hand, the ith subnet of the M-ary RBF equalizer provides the *a posteriori* LP $\mathcal{L}^E_p$ value of the ith coded symbol c^i_k according to

$$\mathcal{L}^E_p\left(c^i_k\right) = \ln\left(\frac{f^i_{RBF}(\mathbf{v_k})}{\sum_{l=1}^{M} f^l_{RBF}(\mathbf{v_k})}\right) \quad (10)$$

where $f^i_{RBF}(\mathbf{v_k})$ was defined by (2), while the term $\sum_{l=1}^{M} f^l_{RBF}(\mathbf{v_k})$ is a normalization factor, ensuring that we have $\sum_{i=1}^{M} \exp(\mathcal{L}^E_p(c^i_k)) = 1$ and the received sequence $\mathbf{v_k}$ is defined in (5).

B. Simulation Results and Discussions

We employed the Jacobian RBF-decision feedback equalizer (DFE) of [11], [28], which reduced the complexity of the RBF equalizer by utilizing the Jacobian logarithmic function [21], and decision feedback assisted RBF-center selection [11], [23] as well as a TEQ scheme using a symbol-based MAP channel decoder. The RBF-DFE-based TEQ is specified by the equalizer's decision delay τ, the feedforward order m and the feedback order n. Specifically, we employed $\tau = 2$, $m = 3$, and $n = 1$. The transmitted $(m - 1)$-bit information symbols are encoded by a rate-$(m - 1)/m$ CM encoder, interleaved and mapped to an M-ary modulated symbol where $M = 2^m$. We utilized 16QAM in order to obtain an effective transmission throughput of $m - 1 = 3$ information bits per symbol (BPS). All the 16QAM-based CM schemes employed exhibited a similar decoding complexity for the sake of a fair comparison. More specifically, a component TCM (or BICM) code memory of 3 was used for the TTCM (or BICM-ID) scheme. The number of iterations for TTCM (BICM-ID) was fixed to 4 (8). Hence, the iterative scheme exhibited a similar decoding complexity to that of the TCM (BICM) code of memory 6 when quantified in terms of the number of coding states [1].

The transmission burst structure used in this system is the FMA1 nonspread data burst specified by the Pan-European FRAMES proposal [29], which is shown in Fig. 3. When considering a time-division multiple-access (TDMA) system having 16 slots per 4.615 ms TDMA frame, the transmission burst length is 288 μs, as shown in Fig. 3. In our investigations, the transmission delay was limited to approximately
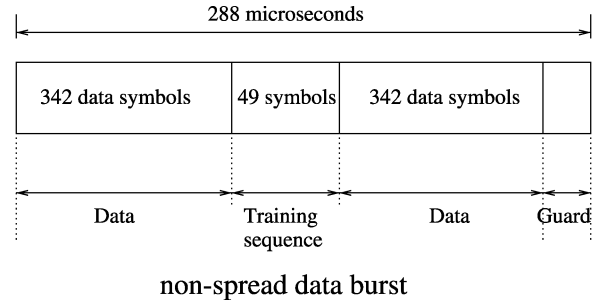

Fig. 3. Transmission burst structure of the FMA1 nonspread speech burst of the FRAMES proposal [29].

8×4.615 ms $= 37$ ms. This corresponds to a transmission delay of 8 TDMA frames and a channel interleaver depth of $8 \times 684 = 5472$ symbols can be employed.

A two-path, symbol-spaced CIR of equal tap weights was used, which can be expressed as $h(t) = 0.707 + 0.707z^{-1}$, where $\bar{L} = 1$ and the Rayleigh-fading statistics obeyed a normalized Doppler frequency of 3.25×10^{-5}. The fading magnitude and phase was kept constant for the duration of a transmission burst, a condition which we refer to as employing transmission burst-invariant fading. The least mean square (LMS) algorithm [30] was employed for estimating the CIR based on the training sequence of the transmission burst, as seen in Fig. 3. Iterative CIR estimation was invoked, where the initial LMS CIR estimation step-size used was 0.05, which was reduced to 0.01 for the second and the subsequent iterations. This LMS-aided CIR estimation was outlined in [11].

Fig. 4 illustrates the BER and FER versus signal-to-noise ratio (SNR) per information bit, namely E_b/N_0 performance of the RBF-TEQ scheme assisted by 16QAM-based TCM, TTCM, BICM, and BICM-ID, when communicating over a dispersive channel having an equally-weighted two-path Rayleigh-fading CIR and utilising iterative LMS-based CIR estimation. The iteration gains of TEQ can be observed by comparing the performance of the first and third TEQ iteration of the systems. The BER and FER performance of the identical-throughput uncoded 8PSK scheme communicating over nondispersive additive white Gaussian noise (AWGN) channels was used as a benchmark for the 16QAM-based RBF-TEQ arrangement using various CM schemes communicating over the aforementioned dispersive Rayleigh-fading channels. We found in Fig. 4 that at a BER of 10^{-5}, the BER curves of the TTCM, BICM, and BICM-ID assisted schemes are only about 2 dB away from the benchmark. However, as seen in Fig. 4, the TCM assisted scheme improves less rapidly than that of the other schemes, partly owing to the existence of unprotected bits in the TCM coded symbols and partly as a consequence of benefiting from no internal iterations. The BER disadvantage of TCM caused by the unprotected bits is overcome by BICM and BICM-ID, since they protect all bits, while TTCM does not, but nonetheless benefits from inner iterations. On the other hand, the FER performance of the TTCM, BICM, and BICM-ID assisted RBF-TEQ schemes was found in Fig. 4 to be better than that of the benchmark at low SNR values. Furthermore, it was found from our simulations that the achievable performance gain remained only marginal when more than three
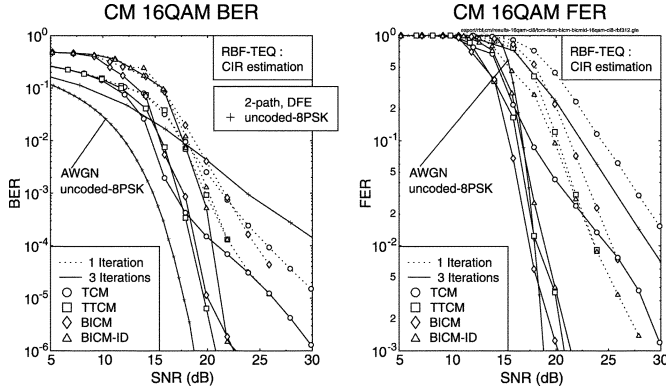
Fig. 4. BER and FER versus E_b/N_0 performance of the RBF-TEQ for various CM 16QAM schemes, when communicating over the dispersive channel having an equally-weighted two-path Rayleigh-fading CIR.

Fig. 5. BPS throughput versus E_b/N_0 performance at BER $= 10^{-5}$ of the RBF-TEQ for various CM 16QAM schemes, when communicating over the dispersive channel having an equally-weighted two-path Rayleigh-fading CIR.
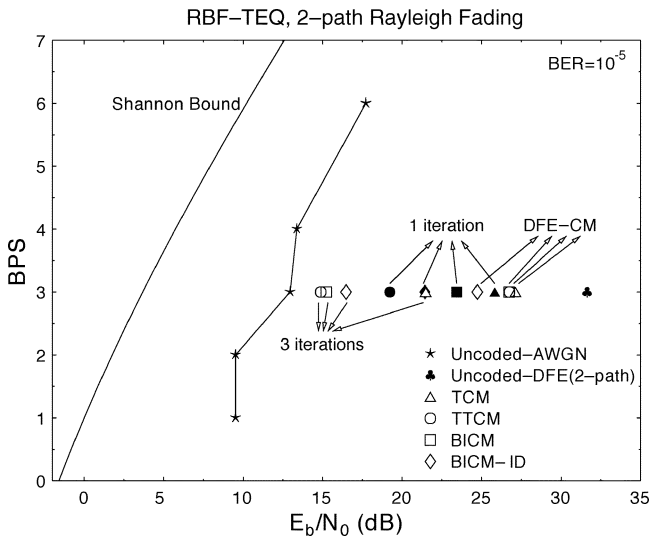
TEQ iterations were employed. It is illustrated in Fig. 4 that the RBF-TEQ-BICM scheme attained the highest TEQ gain compared to its counterparts. The RBF-TEQ-BICM scheme is also the best performer in terms of the achievable FER, but the RBF-TEQ-TTCM arrangement has the edge in terms of the BER attained.

In order to compare the performance of the RBF-TEQ assisted CM scheme to that of the conventional DFE assisted CM scheme, we have plotted in Fig. 5 the BPS throughput versus E_b/N_0 performance of the RBF-TEQ-assisted CM-16QAM scheme at BER $= 10^{-5}$ when employing LMS CIR estimation and that of the conventional DFE assisted CM-16QAM scheme assuming perfect CIR knowledge, when communicating over the two-path Rayleigh-fading channel. The conventional DFE's feedforward order m and feedback order n were set to seven and one, respectively, since we found from our simulations that further increasing the values of m and n yielded no significant performance improvement when communicating over the two-path Rayleigh-fading channel. Specifically, the conventional DFE exhibits a lower complexity than that of the RBF-DFE. However, the BER performance of the conventional DFE scheme is lower than that of its RBF-DFE counterpart

owing to experiencing an error floor in the high SNR region [11]. From Fig. 5, we notice that the conventional DFE assisted CM-16QAM schemes exhibited approximately 4–7 dB coding gain compared to the identical-throughput conventional DFE assisted uncoded-8PSK scheme at a BER of 10^{-5}. However, the achievable coding gain of the various CM schemes was significantly increased when the RBF-TEQ scheme was employed, although this was achieved at a higher complexity owing to employing an increased number of iterations. Explicitly, a coding gain ranging from 10 to 17 dB was achievable at a BER of 10^{-5} by the various CM schemes against the identical-throughput conventional DFE assisted uncoded-8PSK scheme, when the RBF-TEQ scheme used three iterations.

Having studied the performance of the RBF-TEQ arrangement employing various CM schemes, let us now commence our discourse on employing CM schemes in the context of the reduced complexity IQ-TEQ system, to be described in Section IV.

IV. PRINCIPLE OF I/Q EQUALIZATION

We denote the modulated signal by $s(t)$, which is transmitted over the dispersive channel characterized by the CIR $h(t)$. The signal is also contaminated by AWGN $n(t)$ exhibiting a variance of $\sigma^2 = N_0/2$, where N_0 is the single-sided noise power spectral density. The received signal $r(t)$ is then formulated as [11]:

$$\begin{aligned} r(t) &= s(t) * h(t) + n(t) \\ &= [s_I(t) + js_Q(t)] * [h_I(t) + jh_Q(t)] + n_I(t) + jn_Q(t) \\ &= r_I(t) + jr_Q(t) \end{aligned} \tag{11}$$

where we have

$$\begin{aligned} r_I(t) &= s_I(t) * h_I(t) - s_Q(t) * h_Q(t) + n_I(t) \\ r_Q(t) &= s_I(t) * h_Q(t) + s_Q(t) * h_I(t) + n_Q(t) \end{aligned} \tag{12}$$

since the CIR $h(t)$ is complex-valued and, therefore, consists of the I component $h_I(t)$ and Q component $h_Q(t)$. On the same note, $s_I(t)$ and $s_Q(t)$ are the I and Q components of $s(t)$, while $n_I(t)$ and $n_Q(t)$ denote the corresponding AWGN components. Both of the received I/Q signals, namely $r_I(t)$ and $r_Q(t)$ of (12) become dependent on both $s_I(t)$ and $s_Q(t)$ owing to the cross-coupling effect imposed by the channel having a complex CIR. Hence, a conventional channel equalizer, regardless of whether it is an iterative or noniterative equalizer, would have to consider the effects of this cross-coupling.

However, it was shown in [11] that we can compute the I and Q components of the decoupled channel output $r'(t)$, as though they were dependent on $s_I(t)$ or $s_Q(t)$ only, in the context of the following equations [11]:

$$\begin{aligned} r'_I(t) &= r_I(t) + \hat{s}_Q(t) * \hat{h}_Q(t) + j\left[r_Q(t) - \hat{s}_Q(t) * \hat{h}_I(t)\right] \\ &= s_I(t) * h_I(t) + n_I(t) + j[s_I(t) * h_Q(t) + n_Q(t)] \\ &= s_I(t) * h(t) + n'_I(t) \\ r'_Q(t) &= -r_Q(t) + \hat{s}_I(t) * \hat{h}_Q(t) + j\left[r_I(t) - \hat{s}_I(t) * \hat{h}_I(t)\right] \\ &= -s_Q(t) * h_I(t) - n_Q(t) + j\left[-s_Q(t) * h_Q(t) + n_I(t)\right] \\ &= -s_Q(t) * h(t) + n'_Q(t) \end{aligned} \tag{13}$$

where $n'_I(t) = n_I(t) + jn_Q(t)$ and $n'_Q(t) = -n_Q(t) + jn_I(t)$ are the corresponding noise component for $r'_I(t)$ and $r'_Q(t)$, respectively. Note that in (13), we have assumed perfect signal regeneration, i.e., $\hat{s}_I(t) = s_I(t)$ and $\hat{s}_Q(t) = s_Q(t)$, as well as perfect channel estimation, i.e., $\hat{h}_I(t) = h_I(t)$ and $\hat{h}_Q(t) = h_Q(t)$, in order to highlight the underlying principle of the reduced complexity equalizer. More explicitly, the removal of the cross-coupling imposed by the complex CIR is facilitated by generating the estimates $\hat{s}_I(t)$ and $\hat{s}_Q(t)$ of the transmitted signal [22] with the aid of the reliability information generated by the channel decoder and then by cancelling the cross-coupling effects imposed by the channel, yielding $r'_I(t)$ and $r'_Q(t)$, respectively. In the ideal scenario, where perfect knowledge of both the CIR and that of the transmitted signal is available, it is plausible that the channel-induced cross-coupling between the quadrature components can be removed. However, when unreliable symbol estimates are generated owing to the channel-impaired low-confidence reliability values, errors are introduced in the decoupling operation. Nonetheless, we will show that the associated imperfect decoupling effects are compensated with the aid of the iterative TEQ process in its consecutive iterations.

Following the decoupling operation, the modified complex channel outputs, namely $r'_I(t)$ and $r'_Q(t)$ of (13), respectively, can be viewed as the result of convolving both quadrature components independently with the complex CIR on each quadrature arm. Consequently, we can equalize $s_I(t)$ and $s_Q(t)$ independently, hence reducing the number of channel states and the associated complexity quite significantly.

V. RBF ASSISTED REDUCED COMPLEXITY IQ-TEQ OF CODED MODULATION SCHEMES

In the RBF-I/Q-EQ scheme, we utilized the principle of separate I/Q equalization outlined as in Section IV, where two separate RBF equalizers were used for the in-phase and quadrature components of the transmitted symbols. The in-phase-RBF-EQ has RBF centers, which consist of the in-phase decoupled channel output $r'_I(t)$ of (12) and vice-versa for the quadrature-RBF-EQ. The number of possible channel output states is reduced, since the decoupled channel output $r'(t)$ is dependent on $\sqrt{M}$[1] number of possible in-phase or quadrature-phase transmitted symbols instead of the original M number of possible symbols.

A. System Overview

Fig. 6 illustrates the schematic of the turbo equalizer utilising two reduced-complexity RBF-I/Q equalizers. The same notation employed in Section II is used in this section. The subscripts in Fig. 6 are used for representing the iteration index, while the argument within the brackets () indicates the index of the receiver stage, where the equalizers are denoted as receiver stage 0, while the channel decoder as receiver stage 1.

The conventional minimum mean square error (MMSE) DFE seen at the top left corner of Fig. 6 is used for the first TEQ iteration for providing soft decisions in the form of the LP $L_1^p(0)$

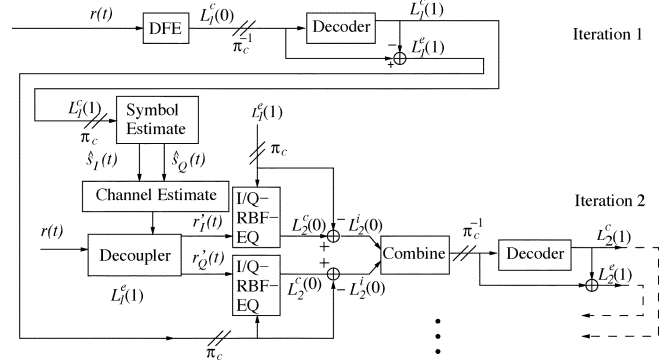[1]Or approximately $\sqrt{M}$ for nonsquare constellations.

Fig. 6. Schematic of the turbo equalizer employing a DFE and a SISO channel decoder in the first TEQ iteration. In subsequent iterations, two RBF-I/Q-EQs and one SISO channel decoder are employed. The notation π_c represents a channel interleaver, while π_c^{-1} is used to denote a channel deinterleaver.

to the CM decoder. Invoking the DFE at the first iteration constitutes a low-complexity approach to providing an initial estimate of the transmitted symbols, as compared to the more complex RBF-I/Q-EQ. The symbol-based MAP channel decoder of Fig. 6 generates the *a posteriori* LP $L_1^p(1)$ and from that, the extrinsic information of the encoded symbols $L_1^e(1)$ is extracted. In the next iteration, the *a posteriori* LP $L_1^p(1)$ is used for regenerating estimates of the I and Q components of the transmitted signal, namely $\hat{s}_I(t)$ and $\hat{s}_Q(t)$, as seen in the "Symbol Estimate" block of Fig. 6. The *a posteriori* information was transformed from the logarithmic domain to modulated symbols using the approach employed in [22]. Furthermore, based on the received signal $r(t)$ and the estimated signals $\hat{s}_I(t)$ and $\hat{s}_Q(t)$, the CIR is estimated in the "Channel Estimate" block to yield $\hat{h}_I(t)$ and $\hat{h}_Q(t)$. The estimated transmitted quadrature components $\hat{s}_I(t)$ and $\hat{s}_Q(t)$ as well as the CIR estimates $\hat{h}_I(t)$ and $\hat{h}_Q(t)$ are then passed to the "Decoupler" block of Fig. 6. At the "Decoupler" block, $\hat{s}_I(t)$ and $\hat{s}_Q(t)$ are convolved with $\hat{h}_I(t)$ and $\hat{h}_Q(t)$ to yield $\hat{s}_I(t)*\hat{h}_I(t)$, $\hat{s}_I(t)*\hat{h}_Q(t)$, $\hat{s}_Q(t)*\hat{h}_I(t)$, and $\hat{s}_Q(t)*\hat{h}_Q(t)$. These resultant outputs are used for removing the cross-coupling effect seen in (12), from both quadrature components of the received signal $r(t)$, yielding $r'_I(t)$ and $r'_Q(t)$, according to (13).

After the decoupling operation, $r'_I(t)$ and $r'_Q(t)$ are passed to the RBF-I/Q-EQ in the schematic of Fig. 6. In addition to these received quadrature signals, the RBF-I/Q-EQ also processes the *a priori* information received, which consists of the extrinsic LPs $L_1^e(1)$ derived from the previous iteration, and generates the *a posteriori* information $L_2^p(0)$. Subsequently, the combined channel and extrinsic information $L_2^i(0)$ is extracted from both RBF-I/Q-EQs in Fig. 6 and combined, before being passed to the Log-MAP channel decoder. As in the first TEQ iteration, the *a posteriori* and extrinsic information of the encoded symbol, namely $L_2^p(1)$ and $L_2^e(1)$, respectively, are evaluated. Subsequent TEQ iterations obey the same sequence of operations, until the iteration termination criterion is met.

B. Simulation Results and Discussions

In this section, we will study the performance of a number of RBF-I/Q-TEQ schemes employing various CM schemes. Similar simulation parameters to those outlined in Section III-B are
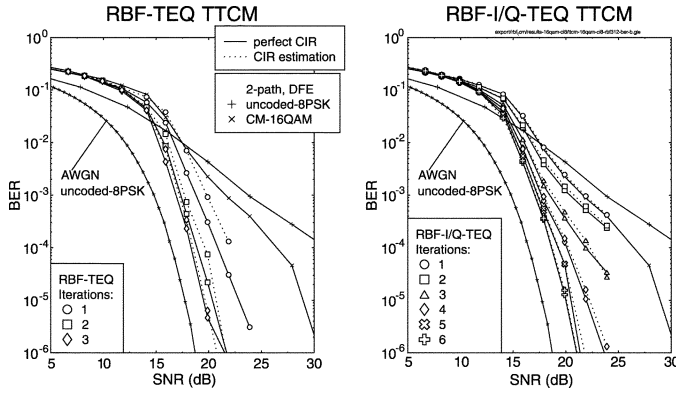
Fig. 7. BER versus E_b/N_0 performance of RBF-TEQ-TTCM and RBF-I/Q-TEQ-TTCM 16QAM schemes, when communicating over the dispersive channel having an equally-weighted two-path Rayleigh-fading CIR.
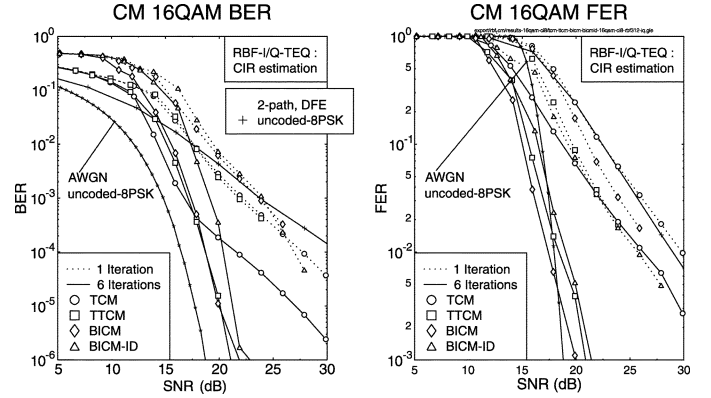

Fig. 8. BER and FER versus E_b/N_0 performance of the RBF-I/Q-TEQ for various CM 16QAM schemes, when communicating over the dispersive channel having an equally-weighted two-path Rayleigh-fading CIR.

used. Again, the RBF-DFE based TEQ is specified by the equalizer's decision delay τ, the feedforward order m and the feedback order n. The number of RBF nodes is $n_{s,i} = \bar{M}^{\bar{L}+m-n}$ and the number of scalar channel states of the Jacobian RBF equalizer is $n_{s,f} = \bar{M}^{\bar{L}+1}$, where we have $\bar{M} = M$ for the non-I/Q-based full-complexity RBF-TEQ system, while $\bar{M} = \sqrt{M}$ for the I/Q based RBF-TEQ system. Again, M is the constellation size and $\bar{L}+1$ is the CIR duration. The estimated computational complexity of generating the *a posteriori* LP for the Jacobian RBF equalizer is given by [28]: $n_{s,i}(m+2) - 2\bar{M} + n_{s,f}$ number of additions/subtractions and $2n_{s,f}$ number of multiplications/divisions. Here, we employed $\tau = 2$, $m = 3$, and $n = 1$ for the RBF-TEQ, as well as $m = 7$ and $n = 1$ for the conventional DFE. Therefore, the "per-iteration" complexity of the full-RBF-TEQ expressed in terms of the number of additions/subtractions and multiplications/divisions is about 20 704 and 512, respectively, while that of the RBF-I/Q-TEQ is about 328 and 32, respectively. Note that in the context of employing 16QAM and communicating over a two-path Rayleigh-fading channel, i.e., when $\bar{L} = 1$, the number of RBF nodes in the RBF-TEQ and RBF-I/Q-TEQ are $M^{\bar{L}+m-n} = 16^3$ and $\sqrt{M}^{\bar{L}+m-n} = 16^{3/2}$, respectively. For the same system, the trellis-based TEQ schemes such as the SOVA or the max-log MAP equalizer would require a computational complexity on the order of $O(16^2)$, which is comparable to that of the RBF-I/Q-TEQ[2] and is $16^3/16^2 = 16$ times lower than that of the RBF-TEQ. Owing to lack of space, the performance of CM-assisted trellis-based TEQ schemes is not studied in this paper.

Fig. 7 illustrates the BER versus E_b/N_0 performance of the RBF-TEQ-TTCM and RBF-I/Q-TEQ-TTCM 16QAM schemes, when communicating over a dispersive channel having an equally-weighted two-path Rayleigh-fading CIR. Our simulation results using perfect CIR estimation are also shown in Fig. 7 for comparison. As we can see at the left of Fig. 7, the RBF-TEQ-TTCM scheme employing LMS-based imperfect CIR estimation, rather than perfect CIR knowledge, exhibited some performance loss compared to an ideal system, but the associated losses reduced rapidly, when the number of TEQ iterations was increased. However, as illustrated at the right of Fig. 7, the RBF-I/Q-TEQ-TTCM scheme employing

LMS-based imperfect CIR estimation exhibited only marginal performance losses compared to the ideal systems employing perfect CIR estimation. This is because the RBF-I/Q-TEQ scheme reduces the effect of error propagation, since the set of RBF centers to be selected using the DFE mechanism is reduced from $\mathcal{M}^n$ to $\mathcal{M}^{n/2}$ [11], [23]. The same observations are also valid for the other CM schemes, although their performance curves were not shown here for reasons of space economy.

Fig. 8 shows the BER and FER versus E_b/N_0 performance of the RBF-I/Q-TEQ for various CM aided 16QAM schemes, when communicating over the dispersive channel having an equally-weighted two-path Rayleigh-fading CIR and utilizing the iterative LMS-based CIR estimation of [11]. Again, the BER performance of the identical-throughput uncoded 8PSK scheme communicating over the nondispersive AWGN channel was used as a benchmark for the 16QAM-based RBF-I/Q-TEQ arrangement using various CM schemes, which communicated over the dispersive two-path Rayleigh-fading channels. It was found from our simulations that the achievable performance gain remained marginal, when more than six TEQ iterations were employed. Explicitly, the first iteration of the RBF-I/Q-TEQ-CM scheme employed a conventional DFE rather than the RBF-DFE, hence the corresponding performance is identical to that of the conventional DFE assisted CM-16QAM schemes. Specifically, the achievable coding gain of the various 16QAM-based RBF-I/Q-TEQ assisted CM schemes against the identical-throughput conventional noniterative DFE assisted uncoded-8PSK scheme increases with the number of iterations. Again, the achievable coding gain of the various RBF-I/Q-TEQ assisted CM schemes is significantly higher than that of the conventional noniterative DFE assisted CM schemes, albeit this is achieved at a higher complexity. Nonetheless, the complexity of the RBF-I/Q-TEQ scheme still remains lower than that of the conventional trellis-based TEQ, as argued in [11], [13].

It is also explicit in Fig. 8 that the RBF-I/Q-TEQ-BICM scheme obtained the highest TEQ gains compared to its counterparts. The RBF-I/Q-TEQ-BICM scheme is also the best performer in terms of the achievable FER, but the RBF-I/Q-TEQ-TTCM scheme is the best performer in terms of the BER attained. Let us now compare the performance of
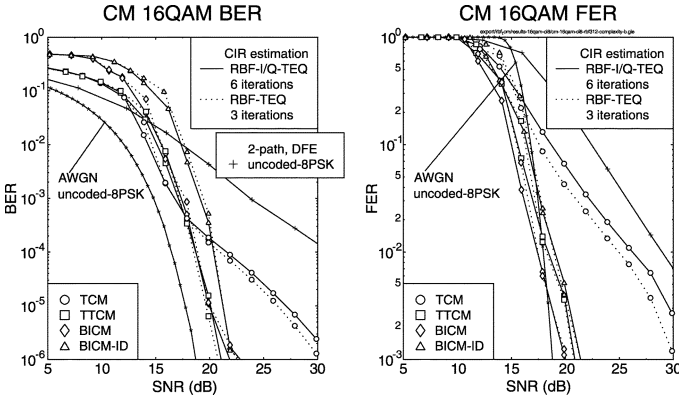
---

[2]The authors would like to thank the anonymous reviewer for this observation.

Fig. 9. BER and FER versus E_b/N_0 performance of the RBF-I/Q-TEQ and RBF-TEQ for various CM 16QAM schemes, when communicating over the dispersive channel having an equally-weighted two-path Rayleigh-fading CIR.

Fig. 10. BER versus E_b/N_0 performance of the RBF-I/Q-TEQ-TTCM and RBF-TEQ-TTCM 16QAM schemes, when communicating over the dispersive channel having an equally-weighted two-path Rayleigh-fading CIR.

the RBF-I/Q-TEQ-CM scheme to that of the RBF-TEQ-CM scheme in Fig. 9. It is found from Fig. 9 that the performance of the RBF-I/Q-TEQ-CM scheme having six iterations is similar to that of RBF-TEQ-CM having three iterations, except for the RBF-I/Q-TEQ-TCM scheme, where the achievable FER performance is about one decibel inferior in comparison to that of the RBF-TEQ-TCM scheme.

Fig. 10 illustrates the BER versus E_b/N_0 performance of the TTCM assisted RBF-I/Q-TEQ and RBF-TEQ schemes on an iteration by iteration basis. In terms of the attainable BER, the performance of the first three iterations of RBF-I/Q-TEQ-TTCM is inferior to that of the first iteration of RBF-TEQ-TTCM for BER values below 10^{-4}. This is due to the employment of a conventional DFE during the first iteration of the RBF-I/Q-TEQ-TTCM scheme, as well as owing to the imperfect I/Q decoupling effects, when unreliable symbol estimates are employed. However, as more reliable symbol estimates become available with the aid of the iterative TEQ scheme during the forthcoming iterations, the performance of RBF-I/Q-TEQ-TTCM becomes comparable to that of the full-complexity RBF-TEQ-TTCM arrangement. Eventually, the performance of RBF-I/Q-TEQ-TTCM having eight iterations is identical to that of RBF-TEQ-TTCM having four iterations for BER values below 10^{-4}, as shown in Fig. 10. Note that the complexity imposed by the conventional DFE during the first RBF-I/Q-TEQ iteration is insignificant compared to that of the remaining RBF-based iterations. Hence, we should compare the complexity of the RBF-DFE assisted scheme using seven iterations in the eight-iteration aided RBF-TEQ-TTCM scheme shown in Fig. 10, to that of the four-iteration full RBF-TEQ-TTCM scheme shown in Fig. 10. Therefore, it can be shown that complexity reduction factors of $(4/7) \cdot (20704/328) \approx 36$ and $(4/7) \cdot (512/32) \approx 9$ were obtained in terms of the required number of additions/subtractions and multiplications/divisions, respectively.

Specifically, as shown in Fig. 10, the 3-BPS throughput RBF-I/Q-TEQ-TTCM scheme employing eight iterations required an E_b/N_0 of about 14.85 dB at BER $= 10^{-5}$ when communicating over dispersive two-path Rayleigh-fading channels. By contrast, the identical 3-BPS throughput uncoded 8PSK AWGN benchmark and the conventional DFE assisted uncoded 8PSK scheme communicating over the dispersive two-path Rayleigh-fading
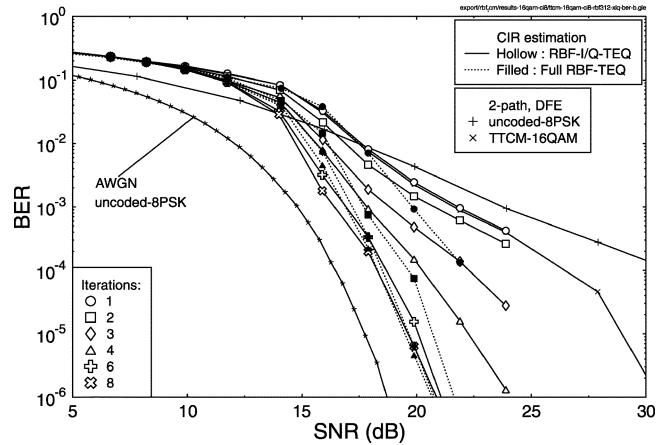
channels required an E_b/N_0 of 12.97 and 31.63 dB, respectively, at BER $= 10^{-5}$. Therefore, the RBF-I/Q-TEQ-TTCM scheme employing eight iterations, required only about $14.85 - 12.97 = 1.88$ dB higher SNR at BER $= 10^{-5}$, than the identical throughput 3-BPS uncoded 8PSK-AWGN benchmark. The coding gain of the scheme is about $31.63 - 14.85 = 16.78$ dB at BER $= 10^{-5}$.

VI. CONCLUSION

The BER performance of both the 16QAM-based RBF-TEQ-CM and RBF-I/Q-TEQ-CM schemes when communicating over wideband-fading channels, was found to be only about 2 dB away from the identical-throughput uncoded 8PSK scheme communicating over AWGN channels. We found that the RBF-I/Q-TEQ scheme employing LMS-based CIR estimation exhibited only marginal performance losses compared to ideal systems employing perfect CIR estimation. This is because the effect of error propagation was reduced significantly when employing RBF-I/Q-TEQ scheme, compared to that of the complex-valued RBF-TEQ scheme.

Our simulation results show significant complexity reductions for the RBF-I/Q-TEQ-CM scheme when compared to complex-valued RBF-TEQ-CM, while achieving virtually the same performance. This was demonstrated in Figs. 9 and 10. Specifically, complexity reduction factors of 36 and 9 were obtained by RBF-I/Q-TEQ-TTCM compared to RBF-TEQ-TTCM, in terms of the required number of additions/subtractions and multiplications/divisions, respectively. Among the four CM schemes, the best performer was TTCM followed by BICM, BICM-ID and TCM in terms of the achievable BER, as shown in Fig. 4 for the RBF-TEQ scheme and in Fig. 8 for the RBF-I/Q-TEQ scheme. However, in terms of the FER attained, the best performer was BICM, followed by TTCM, BICM-ID, and TCM, as was demonstrated in Figs. 4 and 8.

We have also compared the performance of the RBF-TEQ-CM and RBF-I/Q-TEQ-CM schemes to that of the conventional DFE assisted CM scheme, where the coding gain of the RBF-TEQ-CM and RBF-I/Q-TEQ-CM schemes is

significantly higher than that of their conventional DFE-based counterpart, as we have demonstrated in Sections III and V. Although the complexity of RBF-TEQ is higher than that of the conventional DFE, the RBF assisted schemes are capable of maintaining a lower complexity than that of their conventional trellis-based counterparts, when communicating over both dispersive Gaussian- and Rayleigh-fading channels, while maintaining a similar performance [11], [23].

REFERENCES

[1] L. Hanzo, T. H. Liew, and B. L. Yeap, *Turbo Coding, Turbo Equalization and Space Time Coding for Transmission over Wireless Channels*. New York: Wiley, 2002.

[2] G. Ungerböck, "Channel coding with multilevel/phase signals," *IEEE Trans. Inform. Theory*, vol. IT-28, pp. 55–67, Jan. 1982.

[3] P. Robertson and T. Wörz, "Bandwidth-efficient turbo trellis-coded modulation using punctured component codes," *IEEE J. Select. Areas Commun.*, vol. 16, pp. 206–218, Feb. 1998.

[4] E. Zehavi, "8-PSK trellis codes for a Rayleigh-fading channel," *IEEE Trans. Commun.*, vol. 40, pp. 873–883, May 1992.

[5] G. Caire, G. Taricco, and E. Biglieri, "Bit-interleaved coded modulation," *IEEE Trans. Inform. Theory*, vol. 44, pp. 927–946, May 1998.

[6] X. Li and J. A. Ritcey, "Bit-interleaved coded modulation with iterative decoding," *IEEE Commun. Lett.*, vol. 1, Nov. 1997.

[7] S. Chen, S. McLaughlin, and B. Mulgrew, "Complex-valued radial basis function network. Part II: Application to digital communications channel equalization," *EURASIP Signal Processing*, vol. 36, pp. 175–188, Mar. 1994.

[8] L. Hanzo, W. Webb, and T. Keller, *Single- and Multi-Carrier Quadrature Amplitude Modulation*. New York: Wiley, Apr. 2000.

[9] J. G. Proakis, "Communication through band-limited channels," in *Digital Communications*, 3rd ed. New York: McGraw-Hill, Sept. 1995, ch. 10, pp. 583–635.

[10] M. Yee, T. Liew, and L. Hanzo, "Radial basis function decision feedback equalization assisted block turbo burst-by-burst adaptive modems," in *Proc. Vehicular Technology Conf.—Fall*, Amsterdam, The Netherlands, Sept. 19–22, 1999, pp. 1600–1604.

[11] L. Hanzo, C. H. Wong, and M. S. Yee, *Adaptive Wireless Transceivers: Turbo-Coded, Turbo-Equalized and Space-Time Coded TDMA, CDMA and OFDM Systems*. New York: Wiley, 2002.

[12] M. S. Yee, B. L. Yeap, and L. Hanzo, "Turbo equalization of convolutional coded and concatenated space time trellis coded systems using radial basis function aided equalizers," in *Proc. Vehicular Technology Conf.*, Atlantic City, NJ, Oct. 7–11, 2001, pp. 882–886.

[13] ——, "Radial basis function assisted turbo equalization," in *Proc. IEEE Vehicular Technology Conf.*, Tokyo, Japan, May 15–18, 2000, pp. 640–644.

[14] G. Bauch, H. Khorram, and J. Hagenauer, "Iterative equalization and decoding in mobile communications systems," in *Proc. Eur. Personal Mobile Communications Conf.*, Bonn, Germany, Sept. 30–Oct.2 1997, pp. 301–312.

[15] C. Douillard, A. Picart, M. Jézéquel, P. Didier, C. Berrou, and A. Glavieux, "Iterative correction of intersymbol interference: Turbo-equalization," *Eur. Trans. Commun.*, vol. 6, pp. 507–511, 1995.

[16] M. Gertsman and J. Lodge, "Symbol-by-symbol MAP demodulation of CPM and PSK signals on Rayleigh flat-fading channels," *IEEE Trans. Commun.*, vol. 45, pp. 788–799, July 1997.

[17] D. Raphaeli and Y. Zarai, "Combined turbo equalization and turbo decoding," *IEEE Commun. Lett.*, vol. 2, pp. 107–109, Apr. 1998.

[18] C. Berrou and A. Glavieux, "Near optimum error correcting coding and decoding: Turbo codes," *IEEE Trans. Commun.*, vol. 44, pp. 1261–1271, Oct. 1996.

[19] A. Knickenberg, B. L. Yeap, J. Hamorsky, M. Breiling, and L. Hanzo, "Non-iterative joint channel equalization and channel decoding," in *Proc. GLOBECOM*, Rio de Janeiro, Brazil, Dec. 5–9, 1999, pp. 442–446.

[20] L. R. Bahl, J. Cocke, F. Jelinek, and J. Raviv, "Optimal decoding of linear codes for minimizing symbol error rate," *IEEE Trans. Inform. Theory*, vol. 20, pp. 284–287, Mar. 1974.

[21] P. Robertson, E. Villebrun, and P. Höher, "A comparison of optimal and sub-optimal MAP decoding algorithms operating in the log domain," in *Proc. IEEE Int. Conf. Communications*, Seattle, WA, June 1995, pp. 1009–1013.

[22] A. Glavieux, C. Laot, and J. Labat, "Turbo equalization over a frequency selective channel," in *Proc. Int. Symp. Turbo Codes*, Brest, France, Sept. 3–5, 1997, pp. 96–102.

[23] M. Yee and L. Hanzo, "Multi-level radial basis function network based equalizers for Rayleigh channel," in *Proc. IEEE Vehicular Technology Conf.—Spring*, Houston, TX, May 16–20, 1999, pp. 707–711.

[24] S. Chen, B. Mulgrew, and P. M. Grant, "A clustering technique for digital communications channel equalization using radial basis function networks," *IEEE Trans. Neural Networks*, vol. 4, pp. 570–579, July 1993.

[25] S. Chen, B. Mulgrew, and S. McLaughlin, "Adaptive Bavesian equalizer with decision feedback," *IEEE Trans. Signal Processing*, vol. 41, pp. 2918–2927, Sept. 1993.

[26] E.-S. Cling, H. Yang, and W. Skarbek, "Reduced complexity implementation of Bayesian equalizer using local RBF network for channel equalization problem," *Electron. Lett.*, vol. 32, pp. 17–19, Jan. 1996.

[27] S. K. Patra and B. Mulgrew, "Computational aspects of adaptive radial basis function equalizer design," in *Proc. IEEE Int. Symp. Circuits and Systems*, vol. 1, Piscataway, NJ, June 1997, pp. 521–524.

[28] M. S. Yee, T. H. Liew, and L. Hanzo, "Burst-by-burst adaptive turbo-coded radial basis function-assisted decision feedback equalization," *IEEE Trans. Commun.*, vol. 49, pp. 1935–1945, Nov. 2001.

[29] A. Klein, R. Pirhonen, J. Skoeld, and R. Suoranta, "FRAMES Multiple Access MODE 1—Wideband TDMA with and without spreading," in *Proc. IEEE Int. Symp. Personal, Indoor and Mobile Radio Communications*, vol. 1, Helsinki, Finland, Sept. 1–4, 1997, pp. 37–41.

[30] J. G. Proakis, *Digital Communications*, 3rd ed. New York: McGraw-Hill, 1995.

Soon Xin Ng received a first-class B.Eng. degree in electronics engineering and the Ph.D. degree in mobile communications from the University of Southampton, Hampshire, U.K, in 1999 and 2002, respectively.

Currently, he is continuing his research as a Postdoctoral Research Fellow at the University of Southampton. His research interests include adaptive coded modulation, channel coding, turbo coding, space-time coding, and joint source and channel coding. He published numerous papers in these fields.

Mong-Suan Yee received the first-class B.Eng degree in electronics engineering and the Ph.D. degree from the University of Southampton, Hampshire, U.K., in 1996, and 2000, respectively.

Upon graduation, she continued her research as a Postdoctoral Research Fellow for over a year, before joining the Toshiba Research Laboratory, Bristol, U.K. She was later promoted to Senior Research Engineer. Her research interests include neural-network-based algorithms and their application to various wireless communications problems. She coauthored numerous papers and a research monograph in these fields.

Lajos Hanzo (M'91–SM'92–F'03) received the M.S. degree in electronics and the Ph.D. degree from the Technical University of Budapest, Budapest, Hungary in 1976 and 1983, respectively. He received the D.Sc. degree from the University of Southampton, U.K., in 2004.

During his 27-year career in telecommunications, he has held various research and academic posts in Hungary, Germany, and the U.K. Since 1986, he has been with the Department of Electronics and Computer Science, University of Southampton, Hampshire, U.K, where he holds the Chair in telecommunications. Over the years, he co-authored 11 books on mobile radio communications, published in excess of 500 research papers, organized and chaired conferences, presented overview lectures, and been awarded a number of distinctions. Currently, he is managing an academic research team, working on a range of research projects in the field of wireless multimedia communications sponsored by industry, the Engineering and Physical Sciences Research Council U.K, the European IST Programme and the Mobile Virtual Centre of Excellence, U.K. He is an enthusiastic supporter of industrial and academic liaison and he offers a range of industrial courses.

Dr. Hanzo is an IEEE Distinguished Lecturer for both the IEEE Communications and the IEEE Vehicular Technology Societies.